J. Cent. South Univ. (2015) 22: 3837−3848
DOI: 10.1007/s11771-015-2928-5

Springer

Numerical investigations on HCCI engine with increased induction induced swirl and engine speed

T. Karthikeya Sharma, G. Amba Prasad Rao, K. Madhu Murthy

Department of Mechanical Engineering, NIT Warangal-506004(T.S), India

Abstract: Homogeneous charge compression ignition (HCCI) mode of combustion is popularly known for achieving simultaneous reduction of NO_x as well as soot emissions as it combines the compression ignition (CI) and spark ignition (SI) engine features. In this work, a CI engine was simulated to work in HCCI mode and was analyzed to study the effect of induction induced swirl under varying speeds using three-zone extended coherent flame combustion model (ECFM-3Z, compression ignition) of STAR-CD. The analysis was done considering speed ranging from 800 to 1600 r/min and swirl ratios from 1 to 4. The present study reveals that ECFM-3Z model has well predicted the performance and emissions of CI engine in HCCI mode. The simulation predicts reduced in-cylinder pressures, temperatures, wall heat transfer losses, and piston work with increase in swirl ratio irrespective of engine speed. Also, simultaneous reduction in CO_2 and NO_x emissions is realized with higher engine speeds and swirl ratios. Low speeds and swirl ratios are favorable for low CO_2 emissions. It is observed that increase in engine speed causes a marginal reduction in in-cylinder pressures and temperatures. Also, higher turbulent energy and velocity magnitude levels are obtained with increase in swirl ratio, indicating efficient combustion necessitating no modifications in combustion chamber design. The investigations reveal a total decrease of 38.68% in CO_2 emissions and 12.93% in NO_x emissions when the engine speed increases from 800 to 1600 r/min at swirl ratio of 4. Also an increase of 14.16% in net work done is obtained with engine speed increasing from 800 to 1600 r/min at swirl ratio of 1. The simulation indicates that there is a tradeoff observed between the emissions and piston work. It is finally concluded that the HCCI combustion can be regarded as low temperature combustion as there is significant decrease in in-cylinder temperatures and pressures at higher speeds and higher swirl ratios.

Key words: HCCI engine; ECFM-3Z; swirl ratio; emissions and performance

1 Introduction

Internal combustion (IC) engines have become indispensible prime movers over the past one and half century. Though the performance of conventional SI and CI engines is satisfactory, SI engine suffers from poor part load efficiency and high CO emissions. The CI engine yields high particulate and NO_x emissions. These effects may be attributed to their conventional combustion process. Later, a hybrid combustion process called homogeneous charge compression ignition (HCCI) equipped with advanced low-temperature combustion technology gains attention of researchers. In principle, HCCI involves the volumetric auto combustion of a premixed fuel, air, and diluents from low to moderate temperatures and at high compression ratios. The other associated advantages with HCCI mode of combustion have been well documented and presented as a potentially promising combustion mode for internal combustion engines [1−2].

The different combustion models which are well developed for predicting engine processes are transient interactive flamelets (TIF) model, digital analysis of reaction system-transient interactive flamelets model (DARS-TIF), G-equation model [3], extended coherent flame combustion model-3 zones [4] and equilibrium-limited ECFM (ECFM-CLEH) [5−6]. Each model has its own limitations and is suitable for a specific set of problems. Generally speaking, ECFM-3Z and ECFM-CLEH can be used for all types of combustion regime whereas ECFM-3Z is mostly suitable for homogeneous turbulent premixed combustion with spark ignition and compression ignition. Various combustion models' applicabilitis are shown in Table 1. Owing to its wide applicability, in the present work, ECFM-3Z has been used to study the effect of swirl motion of intake charge on emissions and performance of HCCI engine.

Induction induced swirl has a predominant effect on mixture formation and rapid spreading of the flame front in the conventional combustion process of a CI engine. This has been well documented in literatures. However, it is observed that no work has been done on the effect of swirl in HCCI mode. The present study concerns with the analysis of engine pertinent performance parameters by varying the swirl intensity and its effect on the emissions and performance of a CI engine in HCCI

Received date: 2014−11−24; **Accepted date:** 2015−01−13
Corresponding author: T. Karthikeya Sharma, Research scholar; Tel: +91−9912194512; E-mail: karthikeya.sharma3@gmail.com

Table 1 Combustion model applicabilities

Model	Applicability
G-equation	Partially premixed SI and CI
DARS-TIF	Compression ignition
ECFM	Non-homogeneous premixed SI
ECFM-3Z	Premixed and non premixed SI and CI

mode. For this purpose, four swirl ratios between 1 and 4 both inclusive were chosen. The analysis was aimed at studying the parameters like cylinder pressures, temperatures and cylinder wall heat transfer losses, emissions like CO, CO_2, NO_x, and Piston work, turbulent kinetic energy and velocity magnitude. In the present work, emphasis was given on maximizing the piston work and minimizing the NO_x emissions and accordingly the respective optimum swirl ratios were arrived for the chosen engine configuration at varying speeds.

2 Methodology

The software used in the present work makes use of computational fluid dynamics with finite volume approach. The respective governing equations for conservation of mass, momentum, energy and species are solved consecutively in a solver, es-ICE, an expert system developed for internal combustion engines. In the standard k–ε model, the turbulent Reynolds number forms of the turbulent kinetic energy and turbulent dissipation rate equations are used in conjunction with the algebraic 'law of the wall' representation of flow, heat and mass transfer for the near wall region. The ECFM-3Z model is a general purpose combustion model capable of simulating the complex mechanisms of turbulent mixing, flame propagation, diffusion combustion and pollutant emission that characterize modern internal combustion engines. 3Z stands for three zones of mixing, namely the unmixed fuel zone, the mixed gases zone, and unmixed air plus exhaust gas recirculation (EGR) zone. The three zones are too small to be resolved by the mesh and are therefore modeled as sub-grid quantities. The mixed zone is the result of turbulent and molecular mixing between gases in the other two zones and is the zone where combustion takes place. The flame propagation phase is modeled by the flame surface density transport equation incorporating the theoretical flame speed. The engine specifications considered for the analysis are listed in Table 2. The analysis is done from the second cycle after the engine has started.

3 CFD model set-up

The piston bowl shape and 3D mesh of the piston bowl sector is shown in Fig.1. The computational mesh consists of 0.312×10^6 cells. The entire mesh consists of cylinder and 6th portion of the bowl created in Hypermesh, which is a mesh generation utility and imported into STAR-CD for solutions. A spline is developed based on the imported model; 2D template is cut by the spline to cut the 3D mesh with 80 radial cells, 140 axial cells, 5 top dead center layers and 40 axial block cells.

Table 2 Engine specification and operating conditions

Engine specification	Value
Displacement volume/cm^3	1600
Bore/cm	12.065
Stroke/cm	14
Connecting rod length/cm	26
Compression ratio	21:1
Fuel	*n*-Dodecane
Operating condition	**Value**
Engine speed/(r·min^{-1})	1000
Equivalence ratio	0.26
Inlet temperature air, T_{air}/K	353
Inlet air pressure, p_{air}/MPa	0.1
Cylinder wall temperature, T_{wall}/K	450
EGR/%	0

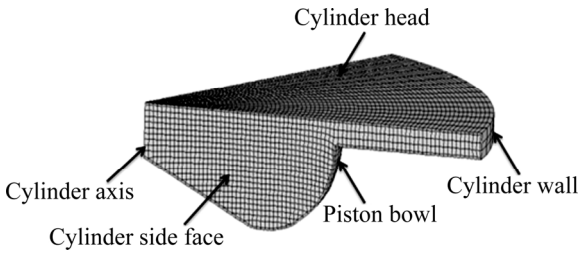

Fig. 1 Schematic representation of 3D piston bowl shape at TDC

Energy efficiency of the engine is analyzed by gross indicated work per cycle (*W*) calculated from the cylinder pressure and piston displacement using

$$W=\frac{\pi aB}{8}\int_{\theta_1}^{\theta_2}p(\theta)\left[2\sin\theta\frac{a\sin(2\theta)}{\sqrt{l^2-a^2\sin^2\theta}}\right]\mathrm{d}\theta \quad (1)$$

where a, l, and B are the crank radius, connecting rod length and cylinder bore, respectively, and θ_1 and θ_2 are the beginning and the end of the valve-closing period.

The indicated power per cylinder (P) is related to the indicated work per cycle by

$$P=\frac{WN}{60000n_r} \quad (2)$$

where n_r=2 is the number of crank revolutions for each

power stroke per cylinder and N is the engine speed (r/min). The indicated specific fuel consumption (ISFC, C_{isf}) is shown as

$$C_{isf}=\frac{30m_{fuel}N}{P} \tag{3}$$

In Eq. (1), the power and ISFC analyses can be viewed as only qualitative rather than quantitative in this work.

4 Modeling process

The STAR-CD used in the present study has integrated several sub models such as turbulence, fuel spray and atomization, wall function, ignition, combustion, NO_x, and soot models for various types of combustion modes in CI as well as SI engine computations. As initial values of k and ε are not known priori the turbulence, initialization is done using I−L model. For this purpose, local turbulence intensity (I) and length scale (L) are related as

$$k_\infty=\frac{3}{2}I^2V_\infty^2 \tag{4}$$

$$\varepsilon_\infty=C_\mu^{3/4}\frac{k_\infty^{3/2}}{L} \tag{5}$$

This practice ensures that k and ε_∞ and the turbulent viscosity μ_t, all scale correctly with V_∞, which is desirable from both the physical realism and numerical stability point of view. Moreover, the turbulent intensity is defined using the same velocity vector magnitude as that of stagnation quantities.

The combustion is modeled using ECFM-3Z. As far as fluid properties are concerned, ideal gas law and temperature dependent constant pressure specific heat (c_p) are chosen.

4.1 Swirl creation

The swirl motion is created by changing the velocities of the intake charge in U and V directions, squish is the radial inward motion that occurs as the piston moves toward TDC, and tumble is created by squish motion and the shape of the clearance volume. U and V components of velocity are calculated by the code using the formulae shown below:

$$U=-(x-x_{CSYS})(\text{Swril}\cdot v_e\cdot 2\pi)/60 \tag{6}$$

$$V=-(y-y_{CSYS})(\text{Swril}\cdot v_e\cdot 2\pi)/60 \tag{7}$$

where U and V are the velocity components of the intake charge in X and Y directions; v_e represents the speed of the engine; x, x_{CSYS}, y and y_{CSYS} represent the coordinates in global and local coordinates of x and y, respectively. The z coordinate of the global and local co-ordinates are matched during modeling and after meshing, which eliminates the errors in swirl creation.

4.2 Spray injection and atomization model

In conventional CI mode, spray and atomization are modeled using Huh's and BAI's model [7−8]. Huh's model considers the two most important mechanisms in spray atomization: gas inertia and the internal turbulence stresses generated in the nozzle. The agitation of jet takes place because of turbulence generated in the nozzle when it exits the hole. Surface wave growth takes place once the agitation of jet reaches a certain limit leading to droplet formation.

The secondary break-up of the droplets is modeled by considering REITZ−DIWAKAR model [9−10]. The REITZ−DIWAKAR model incorporates the droplet break-up due to non-uniform pressure surrounding the droplet (bag break-up) and the other is because of continuous phase (stripping break-up). The occurrence of these regimes is dependent on the magnitude of the droplet incidence Weber number (N_w) and the dimensionless droplet diameter d given as

$$N_w=\frac{\rho_d D_d V_{d,n}^2}{\sigma} \tag{8}$$

where subscript "n" is the unit normal to the wall, ρ_d is the density of the droplet, D_d is the diameter of the droplet, $V_{d,n}$ is the normal component of droplet velocity relative to the wall, and σ is the surface tension coefficient.

For HCCI combustion mode, the premixed reaction mechanism is adopted for the homogeneous fuel air mixture formation.

4.3 Auto ignition model

Ignition delay is computed to establish the ignition occurrence time, instead of the pre-ignition kinetics.

The auto-ignition delay τ_d is calculated based on semi empirical correlations as

$$\tau_d=1.051\times10^{-8}[F]^{0.05}[O_2]^{-0.53}\rho^{0.13}\,e^{5914/T\mu}[47/N_c] \tag{9}$$

where ρ is the density, F is the coefficient value taken from the tables, N_c is the cetane number (maximum of 60). An ignition progress variable function is defined to track the development of the reactions prior to autoignition given as

$$(dY_{igi})/(dt)=Y_{Tf}F(\tau_d) \tag{10}$$

where Y_{igi} is an ignition progress variable function, Y_{tf} is the fuel tracer mass fraction.

For HCCI combustion mode, a double delay autoignition model is used as the autoignition in HCCI

mode controlled by the effect of cool flames. In cool flame regime, the rise in temperature is less and the reaction rates get slowed down. After the second delay, the reaction rate increases, leading to main autoignition. Double-delay autoignition considers two delay times and two ignition progress variables. The delay times are not empirical correlations but obtained from precomputed tables, which can also provide the information about the maximum fuel burnt at each autoignition step.

4.4 Combustion model

A three-zone extended coherent flame combustion model (EFCM-3Z) is used for the analysis. Premixed charge with auto ignition has been considered for the start of combustion. In HCCI engine, the air fuel mixture enters the cylinder like in SI engines, and combustion occurs by compression ignition like in CI engines. Figure 2 depicts the schematic representation of the three zones of the ECFM-3Z model. This model is capable of simulating the complex mechanisms like turbulent mixing, flame propagation, diffusion combustion and pollutant emission that characterize modern IC engines. For the combustion analysis of CI engine in conventional mode turbulent mixing, flame propagation, diffusion combustion models and post flame emission models are used. For HCCI mode mixing model, post flame emissions model and double delay auto ignition models are used.

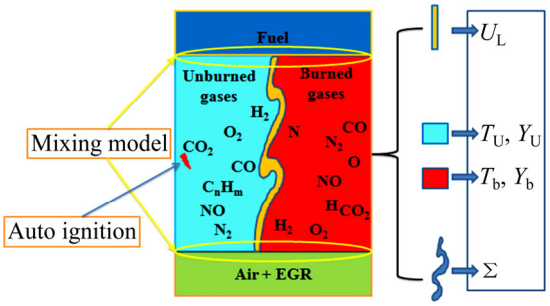

Fig. 2 Schematic representation of three zones of ECFM-3Z model

For wall-bounded flows, most turbulence is generated in the near-wall region. It is therefore necessary to resolve the details of the near-wall flow, which in turn requires a fine mesh in that region. For this, Angelberger wall function model is used [11].

The mixed zone is the result of turbulent and molecular mixing between gases in the other two zones and it is the zone where combustion takes place. The other two zones are characterized by the fuel in the unmixed fuel zone and the species in the unmixed air+EGR zone.

The equations governing the mass fractions of the unmixed fuel (Y_{fum}) is given as:

$$\frac{\partial \rho Y_{fum}}{\partial t}+\nabla\cdot(\rho u Y_{fum})-\nabla\cdot\left[\left(D+\frac{\mu_t}{SC_t}\right)\nabla Y_{fum}\right]=\frac{\beta_{min}}{\pi}Y_{fum}\left(1-Y_{fum}\frac{\rho}{\rho_u}\frac{W_m}{W_f}\right)+\dot{\omega}_e V_e \quad (11)$$

where μ is the molecular viscosity, $\dot{\omega}_e$ is the fraction remaining, V_e is the volume evaporated.

4.5 NO_x model

The high temperatures during the combustion process facilitate the formation of nitrous oxides consisting of NO_2 and NO due to the reaction between the atmospheric nitrogen with oxygen. NO_x emissions are highly affected by the temperature. The higher the combustion temperatures are, the higher the formation of NO_x is. There are two possible sources of nitrous oxide formation in engines, namely, thermal and prompt NO_x. In diesel engines, however, more than 90% of the NO emission stems from the thermal NO formation process. The current approach to model NO production is with the extended Zel'dovich mechanism which consists of the following equations as described by BOWMAN et al [12]

$$O+N_2 \longleftrightarrow NO+N \quad (12)$$

$$N+O_2 \longleftrightarrow NO+O \quad (13)$$

$$N+OH \longleftrightarrow NO+H \quad (14)$$

With the partial equilibrium of Eq. (14) for the hydrogen radicals, it is obtained:

$$O+OH \longleftrightarrow O_2+H \quad (15)$$

The extended Zel'dovich mechanism can be written as a single rate equation for NO, as originally put forth by HEYWOOD [13] given as

$$\frac{d}{dt}[NO]=2k_{1f}[O][N_2]\cdot\left\{\frac{\{1-[NO]^2/K_{12}[O_2]\Sigma d_2\}}{1+k_{1b}[NO]/(k_{2f}[O_2]+k_{3f}[OH])}\right\} \quad (16)$$

where d_2 is the diameter of the droplet in Eq. (13). $K_{12}=(k_{1f}/k_{1b})(k_{2f}/k_{2b})$ and the subscripts 1, 2 and 3 refer to Eqs. (12), (13) and (14), respectively. O, OH, O_2 and N_2 are assumed to be in local thermodynamic equilibrium.

4.6 Soot modeling

Soot formation is the most common process that can be observed during the combustion of fuel-rich hydrocarbons. Fuel pyrolysis and oxidation, formations of polycyclic and aromatic hydrocarbons, and the inception of first particles are the complex reaction reactions that are involved in the formation of soot. A

laminar flamelet model where the scalar quantities are related to scalar dissipation rates and mixture fractions developed by KARLSSON et al [14] is used to model the soot. KARLSSON et al developed a correlation between the rate of soot formation with premixed counter flow flames and local conditions in diffusion flames. In this method, an additional transport equation for the soot mass fraction is solved. Integration of mass fraction space with probability density function is taken to get the soot volume fraction source term from the flamelet library. In order to save computer storage and CPU time, the flamelet library of sources is constructed using a multi parameter fitting procedure resulting in simple algebraic and a proper set of parameters. The transport equation for soot mass fraction is given as

$$\frac{\partial}{\partial t}(\rho Y_{\mathrm{s}})+\frac{\partial}{\partial x_j}(\rho u_j Y_{\mathrm{s}})=\frac{\partial}{\partial x_j}\left(\frac{\mu_t \partial Y_{\mathrm{s}}}{Pr_{\mathrm{t,s}}\partial x_j}\right)+\rho_{\mathrm{s}}\overline{\omega}_v \tag{17}$$

where Y_{s} is the soot fraction, u_j is the absolute fluid velocity component in direction x_j which is the velocity component, the Prandtl number Pr for soot is assumed to be 1.3 and the soot density ρ_{s} is 1860 kg/m^3.

$$\overline{\omega}_{v,i}=\alpha_i\int_0^{\alpha}\int_0^1\frac{1}{f_v}\left(\frac{\partial f_{v,i}}{\partial t}(\hat{f},\hat{\chi})\right)P(\hat{f},\hat{\chi})\mathrm{d}\hat{f}\mathrm{d}\hat{\chi} \tag{18}$$

where $\hat{\chi}$ is the scalar dissipation rate, and α_i is the scaling factor corresponding to each of these effects, which enable the user to scale the rates up or down for sensitivity studies or for calibration purposes. Subscript i="sg", "fr", "ox". In the above equation, "sg" stands for surface growth, "fr" for fragmentation, "ox" for oxidation.

5 Initial and boundary conditions

To begin with, an absolute pressure of 1.02 kPa, 0% EGR, temperature of 353 K, and equivalence ratio of 0.26 are taken as initial values. Fixed boundary wall temperatures are taken with combustion dome regions as 450 K, piston crown regions as 450 K, and cylinder wall regions as 400 K. The Angleberger wall function mode is considered. The two-layer and low Reynolds number approach, where no-slip conditions are applied directly and the boundary layers are computed by solving the mass, momentum and turbulence equations (the latter in their low Reynolds number form) within them [15]. The hybrid wall boundary condition which is a combination of two layered and low-Reynolds number wall boundary conditions is considered in this analysis. This hybrid wall boundary condition removes the burden of ensuring a small enough near-wall value for y^+ (by creating a sufficiently fine mesh next to the wall). The y^+ independency of the hybrid wall condition is achieved using either an asymptotic expression valid for $0.1<y^+<100$ or by blending low-Reynolds and high-Reynolds number expressions for shear stress, thermal energy and chemical species wall fluxes and y^+ for the near-wall cell should be of the order of 1.0. This treatment provides valid boundary conditions for momentum, turbulence, energy and species variables for a wide range of near-wall mesh densities.

Standard wall functions are used to calculate the variables at the near wall cells and the corresponding quantities on the wall. The initial conditions are specified at inlet valve closing, consisting of a quiescent flow field at pressure and temperature for full load condition.

6 Validation of ECFM-3Z, compression ignition model

STAR-CD is a well known commercial CFD package adopted by many renowned researchers and is well established by research organizations in the field of automotive IC engines. The results obtained through this package are validated with the experimental results by many researchers [16−18]. A comparison of the CI engine in HCCI is done in this work considering the extended coherent flame combustion three zones, compression model for combustion analysis. The present work deals with the simulation of CI engine in HCCI mode, using a fuel vaporizer to achieve excellent HCCI combustion in a single cylinder air-cooled direct injection diesel engine. No modifications are made to the combustion system. GANESH and NAGARAJAN [19] conducted experiments with diesel vapor induction without EGR and diesel vapor induction with 0%, 10% and 20% EGR. Validation of the present model with GANESH's experimental results is done considering all the engine specifications.

In previous work, a vaporized diesel fuel is allowed to mix with air to form a homogeneous mixture and inducted into the cylinder during the intake stroke. To control the early ignition of diesel vapor and air mixture, cooled (30 °C) EGR technique is adopted. For the validation purpose, the results are compared with respect to engine performance and emissions. It is observed that the simulated results are in good agreement with the experimental results. The comparison of the plots between simulation and experimental results is shown in Fig. 3. As shown, EDVI represents the experimental diesel vapor injection, SDVI represents simulated diesel vapor induction at respective EGR concentrations. EDDI represents the experimental direct diesel injection, and SDDI represents the simulated direct diesel injection.

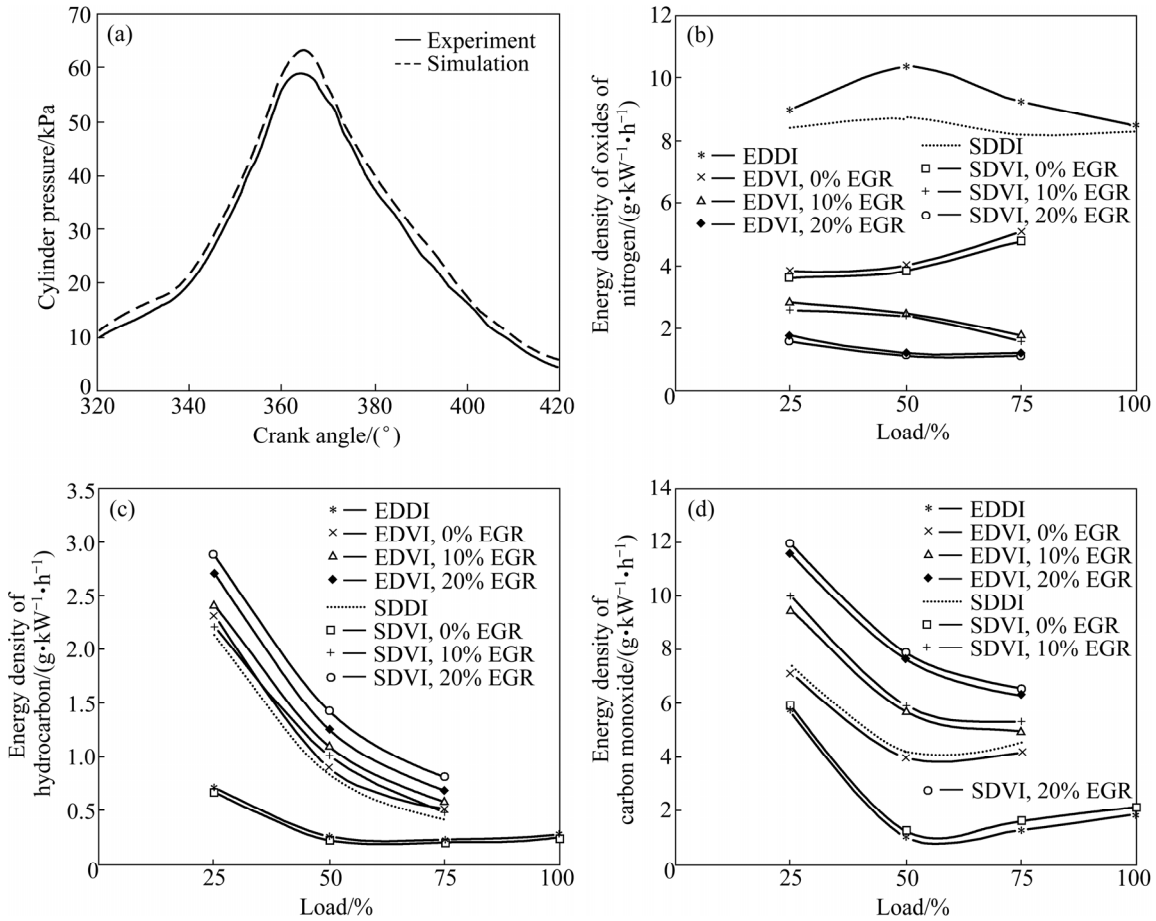

Fig. 3 Validation of ECFM-3Z compression ignition model with experimental results of external mixture formation of HCCI engine: (a) Cylinder pressure vs crank angle; (b) Energy density of NO_x vs load; (c) Energy density of hydrocarbon vs load; (d) Energy density of CO vs load

7 Results and discussion

The effects of swirl motion on the performance of HCCI engine with diesel as fuel are studied with swirl ratios ranging from 1 to 4. Analysis of the effect of swirl ratio on a single cylinder HCCI engine is simulated, using a three-zone extended coherent flame (ECFM-3Z) CFD model. The results are plotted and discussed below.

7.1 In-cylinder pressures

The variation of in-cylinder pressures of the reentrant piston bowl with varying engine speed using swirl ratio of 1 is plotted in Fig. 4. The in-cylinder pressure decreases with the increase in engine speed irrespective of the swirl ratio [20]. The decrease of in-cylinder pressures is due to less residence time available for the burnt gasses at higher speeds which could not release their energy in short time. The reduction in in-cylinder pressures is also obtained at higher swirl ratios. With the increase in swirl ratio, there is a turbulence that enhances the wall heat transfer losses.

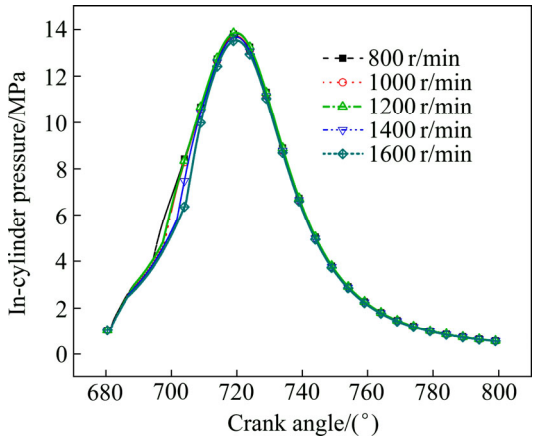

Fig. 4 In-cylinder pressure vs crank angle at swirl ratio of 1

The variation of wall heat transfer losses with swirl ratio is illustrated in Fig. 5. It can be observed clearly that wall heat transfer losses increase with the increase in speed at all swirl ratios. From Fig. 4, it can be seen that in-cylinder pressures at 1200 r/min are higher compared to those at other speeds at a swirl ratio 1. Maximum in-cylinder pressures of 13.714 MPa at 719.825° and 13.53 MPa at 719.825° are obtained at 800 r/min and 1600

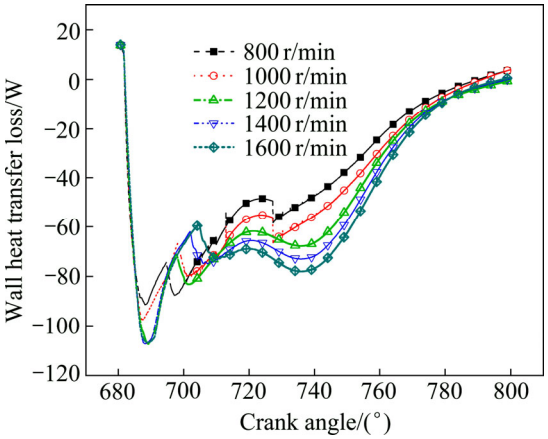

Fig. 5 Wall heat transfer loss vs crank angle at swirl ratio of 1

r/min, respectively. A total decrease of 1.36% in in-cylinder pressures is obtained when the speed increases from 800 to 1600 r/min.

7.2 In-cylinder temperatures

The major amount of the turbulence has resulted in increased heat loss to observed the cylinders walls without contributing to the piston wall but drop is observed at the in-cylinder pressures and temperatures. Figure 6 shows the variation of in-cylinder temperatures with speed at swirl ratio of 4. It can be seen that the temperature decreases with the increase in speed irrespective of the swirl ratio. This is due to the fact that with the increase in speed, the time required for the release of energy gets reduced, which in turn reduces the temperatures. Also, increased swirl ratios enhance the wall heat transfer losses with increasing turbulence as swirl ratio increases. The increased turbulence in the combustion chamber with swirl ratio facilitates towards the well homogeneous mixture formation, and this leads towards the ideal volumetric combustion, causing low temperature combustion. Increases in speed and wall heat transfer losses are the secondary reason for the reduced peak temperatures. A maximum in-cylinder temperatures of 1186.654 K at 719.25° and 1160.34 K at 720.475° are obtained at 1200 r/min and 1600 r/min, respectively. A total decrease of 2.27% in in-cylinder temperatures is obtained when the speed increases from 800 to 1600 r/min.

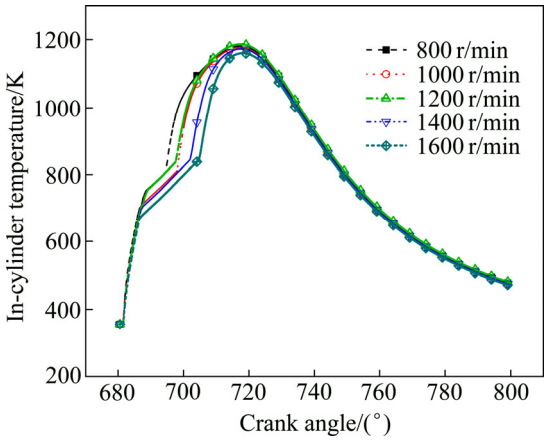

Fig. 6 In-cylinder temperature vs crank angle at swirl ratio of 4

7.3 CO and CO_2 emissions

In-cylinder temperatures play a major role in the formation of emissions. Higher in-cylinder temperatures facilitate the conversion of CO to CO_2 and lower temperatures reduce the formation of NO_x. A clear reduction from 1186.654 K at 719.25° to 1160.34 K at 720.475° is obtained at 1200 and 1600 r/min, respectively, as shown in Fig. 6. Usually, CO emissions increase with the increase in swirl ratio; similar trend is observed with the increase in speed [21]. Figure 7 represents variation of CO emissions with speed at swirl ratio of 1. The reason for increase in CO emissions is due to incomplete oxidation because of low temperatures prevailed in HCCI mode. Also, a reduction of in-cylinder temperatures and increased wall heat transfer losses with increase in engine speed is responsible for increased CO emissions along with the incomplete combustion because of the lack of time for proper combustion at high speeds. CO emissions of 0.19 g/kg fuel and 0.141 g/kg fuel are obtained when the engine runs at 800 and 1600 r/min with swirl ratio of 4. A total increase of 15.6% in CO emissions is obtained when the speed of the engine increases from 800 to 1600 r/min. These emission values are observed to be low compared with the CO emissions at swirl ratio of 4 at all speeds.

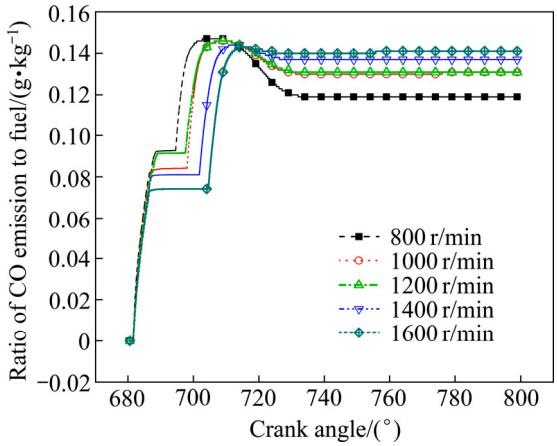

Fig. 7 CO emission vs crank angle at swirl ratio of 1

The variation of CO_2 emissions with speed at swirl ratio of 4 is shown in Fig. 8. The decrease in CO_2 emissions with the increase in engine speed at higher swirl ratio is due to the reduced in-cylinder temperatures and increased wall heat transfer losses not facilitating the

conversion of CO to CO_2 by reacting O_2 available. CO_2 emissions of 0.0674 g/kg fuel and 0.486 g/kg fuel are obtained when the engine speed increases from 800 to 1600 r/min at swirl ratio of 4. A total decrease of 38.68% in CO_2 emissions is obtained when the engine speed increases from 800 to 1600 r/min at swirl ratio of 4. The CO_2 emissions obtained at swirl ratio of 4 are lower when being compared with those at swirl ratio of 1.

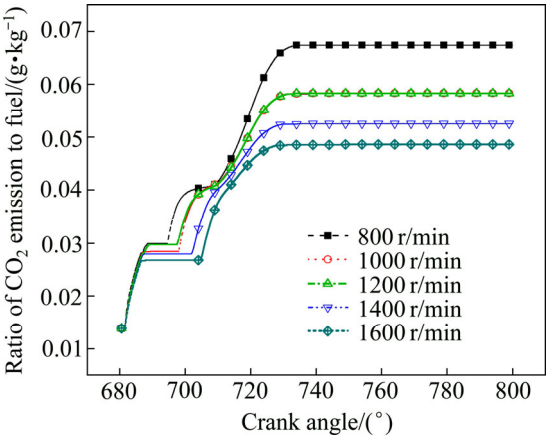

Fig. 8 CO_2 emission vs crank angle at swirl ratio of 4

7.4 NO_x emissions

The formation of NO_x is highly dependent on the in-cylinder temperatures, oxygen concentration and residence time for the reaction to take place. As the in-cylinder temperatures have not increased with swirl intensity, significant reduction in NO_x emissions with increase in swirl is obtained, as shown in Fig. 9. Another reason for the reduced NO_x emission is the detaining of the oxidation of the atmospheric N_2 to react with the available O_2 to form NO_x, which usually occurs at high temperatures [22]. Irrespective of reduced NO_x emissions with the increase in swirl ratio, similar trends are observed with the increase in speed at all swirl ratios. This concludes that higher swirl ratios and higher speeds are favorable for low NO_x emissions. NO_x emissions of

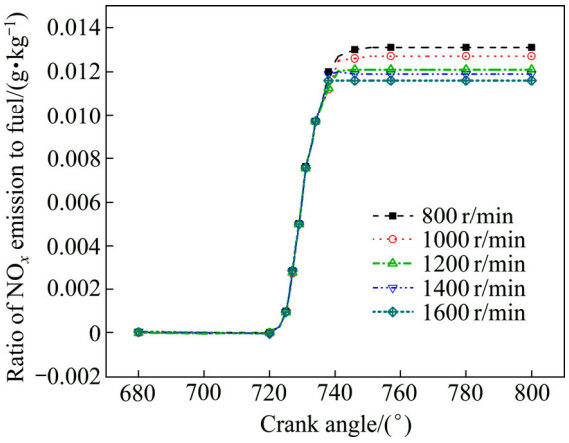

Fig. 9 NO_x emission vs crank angle at swirl ratio of 4

0.00131 g/kg fuel and 0.00116 g/kg fuel are obtained when the engine runs at 800 and 1600 r/min at swirl ratio of 4. A total decrease of 12.93% in NO_x emissions is obtained when the engine speed increases from 800 to 1600 r/min at swirl ratio of 4. The NO_x emissions obtained at swirl 4 are low when compared with those at swirl ratio of 1.

7.5 Piston work

Piston work of an IC engine represents the load bearing capability of the engine. Figure 10 represents the piston work vs crank angle of the HCCI engine under different engine speeds with swirl ratio of 1. The initial decrement in piston work represents the work spent in suction and compression strokes (work done on the piston) and the later increase in piston work represents the work done by the piston. Also, the increase in wall heat transfer losses with the increase in swirl ratio decreases the piston work. Increase in piston work is observed with the increase in engine speed at all the swirl ratios in spite of higher wall heat transfer losses and decreased in-cylinder pressures. It can be concluded that higher engine speeds and low swirl ratios are favorable to get higher piston work. Variation in piston work with engine speed at swirl ratio of 1 can be seen from Fig. 10. It is observed that the improvement in the piston work between any two consecutive swirl ratios is marginal. However, an increase of 14.16% in net work done is obtained with the engine speed increasing from 800 to 1600 r/min at swirl ratio of 1.

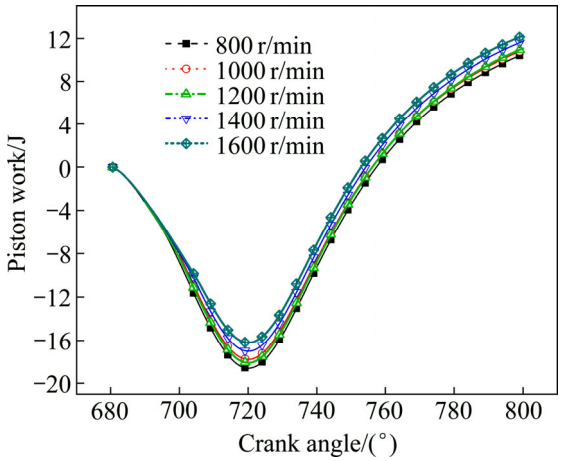

Fig. 10 Piston work vs crank angle at swirl ratio of 1

7.6 Turbulent kinetic energy

Turbulent kinetic energy is an important parameter to determine the burn time and flame speed at a particular region [23]. The turbulence controls the flow dissipation rate, flame propagation rate and heat transfer and it is quantified by turbulent kinetic energy within the

cylinder. The regions with low turbulent kinetic energy represent relatively long time for the flame front to disappear. Turbulent kinetic energy depends on the kinematic viscosity. The kinetic energy of the incoming flow contributes to the turbulent kinetic energy within the cylinder. Figure 11 shows the variation of turbulent kinetic energy with engine speed concentration at different crank angles with swirl ratio of 4. It is found that with the increase in swirl ratio, the turbulent kinetic energy also increases. It is evident from Fig. 11 that the turbulent kinetic energy increases with the increase of speed at all swirl ratios. The increase in turbulent kinetic energy is a clear indication of the improved combustion and faster burn time leading towards a perfect volumetric combustion which is the the important characteristic of HCCI combustion [24].

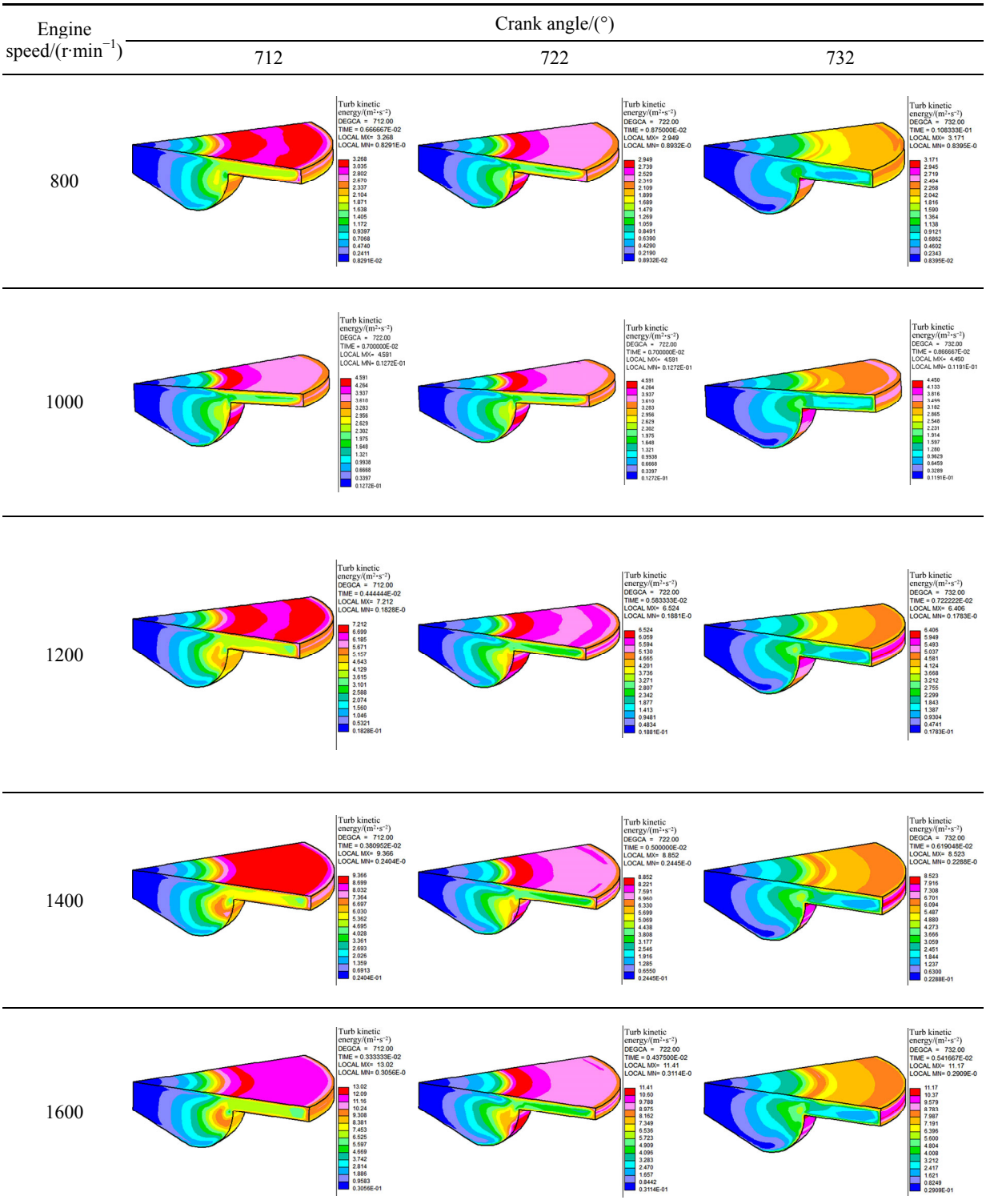

Fig. 11 Variations of turbulent kinetic energy with engine speed at various crank angels at swirl ratio of 4

7.7 Velocity magnitude

Whether the combustion process is efficient or not is understood by velocity magnitude of the combustion chamber. It provides regions of incomplete combustion and necessitates improvement for incorporating efficient combustion [25]. The poor velocity regions in combustion volume represent poor mixing of the fuel and air leading to incomplete combustion [26], which shows the need for better combustion chamber designs to create proper turbulence for the better mixture formation. From Fig. 12, it can be observed that with increase in swirl ratio the velocity magnitude increases irrespective of the engine speed. Similar trends are observed with the increase in speed at all swirl ratios.

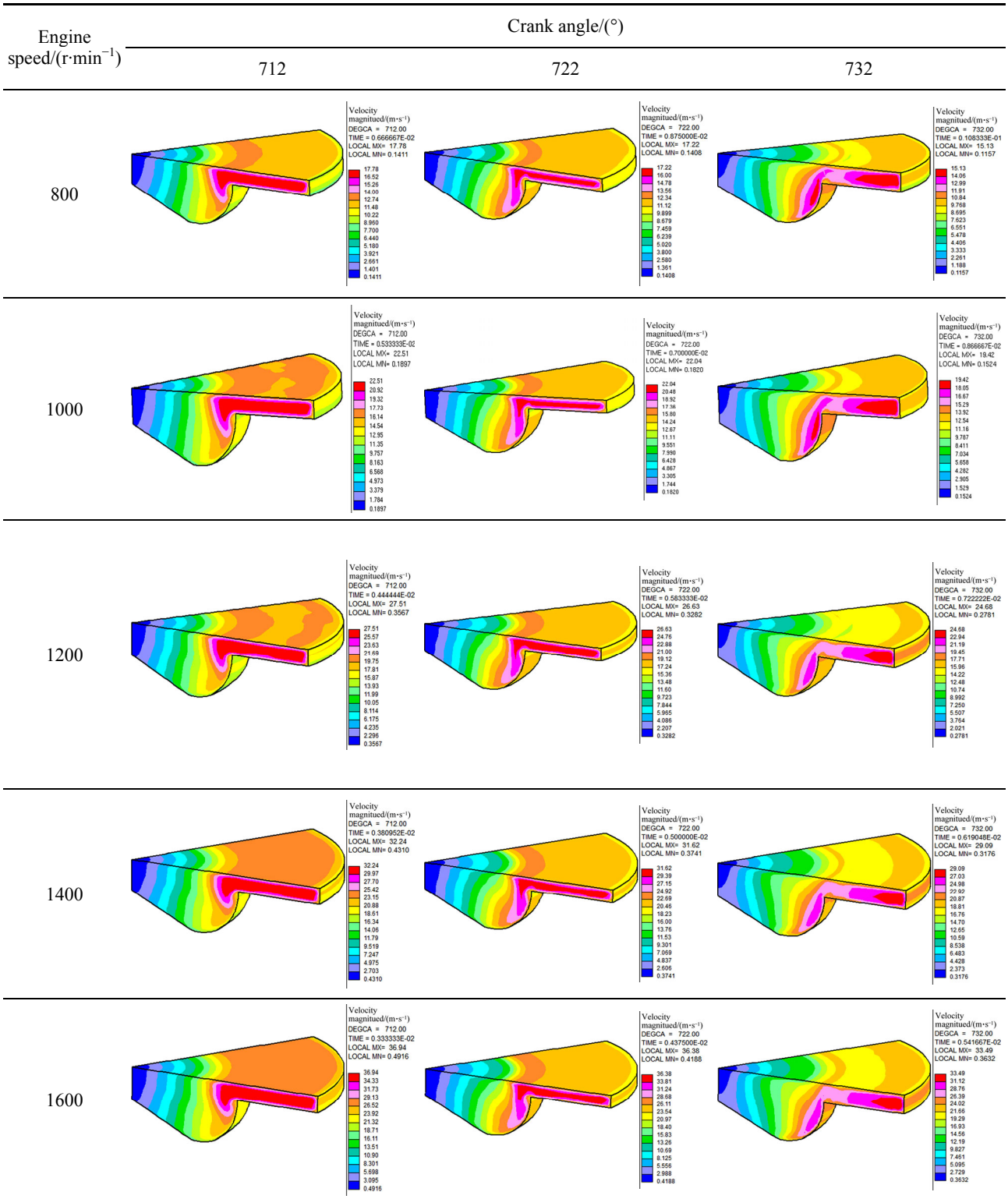

Fig. 12 Variation of velocity magnitude with engine speed at various crank angels at swirl ratio of 4

But higher speeds and swirl ratios are favorable for higher velocity magnitudes. Figure 12 shows the velocity magnitude variation with crank angle at different speeds. It is clear from Fig. 12 that the velocity magnitude gets increased with swirl ratio, leading to better combustion. The results reveal that better velocity magnitudes representing better combustion can be achieved by increasing the swirl ratio without modifying the combustion chamber shape.

8 Conclusions

Predictions of engine performance under four swirl ratios with increase in engine are done using extended coherent flame combustion analysis considering three zones. Based on the work, the following conclusion are arrived.

1) ECFM-3Z of STAR-CD well predicts the performance and emissions of CI engine in HCCI mode. It is observed that swirl ratio is a major factor in achieving HCCI mode of combustion with significant reduction in harmful NO_x emissions. Decrease in residence time for release of energy and increased wall heat transfer losses are observed to be the major causes for the decrease of in-cylinder pressures and temperatures at higher speeds and higher swirl ratios, respectively. Prevalence of low in-cylinder temperatures is observed to be the reason behind the increase in CO emissions and decrease in NO_x emissions at all swirl ratios and speeds.

2) It is revealed that there is a tradeoff between emissions and piston work at higher speeds and lower swirl ratios. Lower speeds and swirl ratios favor the oxidation of CO to form CO_2 so the CO emissions reduce and CO_2 emissions get increased. Higher speeds and higher swirl ratios favor low CO_2 emissions. Significant reduction in NO_x emission is observed at higher speeds and swirl ratios. The reduction in NO_x emissions is achieved by scarifying a little amount of piston work. Higher swirl ratio results in faster burn process and volumetric combustion with increased turbulent kinetic energy and velocity magnitude levels within the combustion chamber.

3) HCCI combustion can be regarded as low temperature combustion as there is significant decrease in in-cylinder temperatures and pressures at higher speeds and higher swirl ratios.

Acknowledgements

The authors would like to thank Dr. Raja Banerjee, Associate Professor, IIT Hyderabad for allowing to use computational facility, Mr. B. Siva Nageswara Rao from CD-adapco, Bengaluru and Mr. P. Madhu computer lab supervisor IIT Hyderabad for their support during the simulation work.

References

[1] NAJAFABADI I M, ABDUL N A. Homogeneous charge compression ignition combustion: Challenges and proposed solutions [J]. Journal of Combustion, 2013, Doi.10.1155/2013/783789.

[2] SHARMA T K, RAO G A P, MADHU M K. Effect of swirl on performance and emissions of CI engine in HCCI mode [J]. Journal of the Brazilian Society of Mechanical Sciences and Engineering, 2014, DOI: 10.1007/s40430-014-0247-7.

[3] CIPOLLA G, VASSALLO A, CATANIA A E, EZIO S, STAN C, DRISCHMANN L. Combined application of CFD modeling and pressure-based combustion diagnostics for the development of a low compression ratio high-performance diesel engine [J]. SAE Technical Paper, No. 2007-24-0034.

[4] COLIN O, BENKENIDA A. The 3-zone extended coherent flame model (ECFM3Z) for computing premixed/diffusion combustion [J]. Oil & Gas Science and Technology–Rev. IFP, 2004, 59(6): 593−609.

[5] RAVET F, ABOURI D, ZELLAT M, DURANTI S. Advances in combustion modeling in STAR-CD: Validation of ECFM CLE-H model to engine analysis [C]// 18th Int Multidimensional Engine Users' Meeting at the SAE Congress. Detroit, 2008: 1−6.

[6] SUBRAMANIAN G, VERVISH L, RAVET F. New developments in turbulent combustion modeling for engine design: ECFM-CLEH combustion submodel [J]. SAE International, No. 2007-01-0154.

[7] HOSSAINPOUR S, BINESH A R. Investigation of fuel spray atomization in a DI heavy-duty diesel engine and comparison of various spray breakup models [J]. Fuel, 2009, 88(5): 799−805.

[8] BAI C, GOSMAN A D. Development of methodology for spray impingement simulation [J]. SAE Technical Paper, No. 950283-1995.

[9] REITZ R D, DIWAKAR R. Structure of high-pressure fuel spray [J]. SAE Technical Paper Series, SAE Paper No. 870598-1987.

[10] REITZ R D, DIWAKAR R. Effect of drop breakup on fuel sprays [J]. SAE Technical Paper Series, SAE Paper No. 860649-1986.

[11] ANGELBERGER C, POINSOT T, DELHAY B. Improving near-wall combustion and wall heat transfer modeling in SI engine computations [J]. SAE Technical Paper, No. 972881-1997.

[12] BOWMAN E J, SIEBERS A, ALTENDORF K. Bafilomycins: A class of inhibitors of membrane ATPases from microorganisms, animal cells, and plant cells [J]. Proceedings of the National Academy of Sciences, 1988, 85(21): 7972−7976.

[13] HEYWOOD J B. Internal combustion engine fundamentals [M]. New York: McGraw-Hill Company, 1988.

[14] KARLSSON A, MAGNUSSON I, BALTHASAR M, MAUSS F. Simulation of soot formation under diesel engine conditions using a detailed kinetic soot model [J]. SAE Technical Paper, No. 981022-1998.

[15] MOUREAU V, LARTIGUE G, SOMMERER Y, ANGELBERGER C, COLIN O, POINSOT T. Numerical methods for unsteady compressible multi-component reacting flows on fixed and moving grids [J]. Journal of Computational Physics, 2005, 202(2): 710−736.

[16] VENKATESWARAN S P, NAGARAJAN G. Effects of the Re-entrant bowl geometry on a DI turbocharged diesel engine performance and emissions—A CFD approach [J]. Journal of Engineering for Gas Turbines and Power, 2010, 132(2): 1113−1122.

[17] MARC Z, DURANTI S, LIANG Yong-jun, KRALJ C, SCHMIDT G, DUCLOS J M. Towards a universal combustion model in STAR-CD for IC engines: From GDI to HCCI and application to DI diesel combustion optimization [C]// Proceeding of 14th International Multidimensional Engine User's Meeting, SAE Cong. 2005: 1−8.

[18] BAKHSHAN Y, TARAHOMI A R. Multi-dimensional simulation of n-heptane combustion under HCCI engine condition using detailed chemical kinetics [J]. Journal of Engine Research, 2011, 22: 3−12.

[19] GANESH D, NAGARAJAN G. Homogeneous charge compression ignition (HCCI) combustion of diesel fuel with external mixture formation [J]. Energy, 2010, 35(1): 148−157.

[20] ANNARITA V, MAGI V. A comprehensive investigation on the emissions of ethanol HCCI engines [J]. Applied Energy, 2012, 93: 277−287.

[21] DEMBINSKI H W R, HANS-ERIK A. Optical study of swirl during combustion in a CI engine with different injection pressures and swirl ratios compared with calculations [J]. SAE Technical Paper, No. 2012-01-0682.

[22] MAGNUS S, DEC J E. Effects of engine speed, fueling rate, and combustion phasing on the thermal stratification required to limit HCCI knocking intensity [J]. SAE Technical Paper, No. 2005-01-2125.

[23] GU Yong-xian, MAYOR J R, DAHM W J A. Turbulence-augmented minimization of combustion time in mesoscale internal combustion engines [C]// 44th AIAA Aerospace Sciences Meeting and Exhibit. AIAA, 2006: 16293−16312.

[24] KURNIAWAN H W, SHAHRIR A, KAMARUZZAMAN S, ZULKIFLI M N, AZHARI S. CFD investigation of fluid flow and turbulence field characteristics in a four-stroke automotive direct injection engine [J]. Journal of Institution of Engineers, 2008, 69(1): 1−12.

[25] KRISHNA B M, MALLIKARJUNA J M. Effect of engine speed on in-cylinder tumble flows in a motored internal combustion engine−An experimental investigation using particle image velocimetry [J]. Journal of Applied Fluid Mechanics, 2011, 4(1): 1−14.

[26] GORYNTSEV D, SADIKI A, KLEIN M, JANICKA J. Large eddy simulation based analysis of the effects of cycle-to-cycle variations on air–fuel mixing in realistic DISI IC-engines [J]. Proceedings of the Combustion Institute, 2009, 32(2): 2759−2766.

(Edited by FANG Jing-hua)